forum acusticum 2026
8-12 September · Graz, Austria

CONTRIBUTION OF FEEDBACK COMPONENTS TO THE INSTABILITY OF REVERBERATION ENHANCEMENT SYSTEMS: A CASE STUDY

Gian Marco De Bortoli[1], Karolina Prawda[2], Tapio Lokki[1], Sebastian J. Schlecht[3]

[1] *Acoustics Lab, Department of Information and Communications Engineering, Aalto University, Finland*
[2] *School of Physics, Engineering, and Technology, University of York, UK*
[3] *Multimedia Communications and Signal Processing, Friedrich-Alexander-Universität Erlangen-Nürnberg, Germany*

This paper is a revised version of the authors' submitted manuscript that was peer-reviewed by at least two anonymous reviewers.

Abstract

Reverberation enhancement systems (RESs) are designed primarily for large concert halls, in which case the energetic and statistical properties of the feedback paths have been extensively studied. However, RESs are also used in smaller and less reverberant spaces, where room acoustic parameters differ from concert halls'. As the stability threshold, or gain-before-instability (GBI), of a RES is commonly estimated via in-situ measurements, the room acoustic properties and transducer setup may greatly influence such analysis. However, the literature does not properly discuss the extent of that effect for non-concert-hall venues, nor it offers guidance on the choice of a stability-improvement technique based on the feedback analysis. This work explores the individual impact of direct sound, early reflections, and late reverberation on GBI estimation in a medium-sized dry venue in octave bands. The comparison with the usual approach of analyzing the entire response shows how the contributions of the three components vary according to the system setup. This work aids in the systematic analysis of RESs for medium and small venues, challenging assumptions regarding reverberant field and GBI estimation, and tackles the improvement of stability based on RES topology.

Keywords: *virtual acoustics, system stability, room acoustics*

1. Introduction

Any audio event, whether speech or music, has its own needs from the acoustical properties of the hosting venue. Through real-time active control of the reverberant field in enclosed spaces, reverberation enhancement systems (RESs) allow rooms to adapt to the specific audio event [1]. They record sound sources with microphones, enhance the time-frequency content of signals with a digital signal processor (DSP), and play back the enhanced audio through loudspeakers. This process builds an artificial reverberant field on top of the room natural reverberation.

Originally, RESs were designed for concert halls to inject energy at low-energy frequencies and to provide an alternative to passive variable-acoustic methods [2]. Although the multipurpose design of concert halls remains the main application of RESs, several other use cases have received interest over the years, such as rehearsal spaces [3], [4], recording studios [5], [6], and outdoor installations [7], [8]. All of these spaces differ from concert halls in terms of size and reverberation properties.

Due to the presence of microphones and loudspeakers in the same space, RESs suffer from feedback, which can lead to instability. The estimation of the stability threshold is important, as it sets the safety limit for the output levels of the loudspeakers: the gain-before-instability (GBI). The literature discusses two stability analysis methods: one is deterministic [9], [10], [11] and one is statistical [12], [13], [14]. The former method is based on in-situ measurements and supported by known feedback stability criteria [15], [16]. The latter is based on the diffuse-field assumption, assuming known statistical properties of the feedback RIRs [17].

There are two main RES topologies: regenerative and in-line [1], [18]. Regenerative systems use ambient microphones distributed throughout the entire room. They make use of feedback to enhance the room reverberation. In large concert halls the natural reverberation is rich and the reverberation time is long, thus these systems typically employ DSPs with

Corresponding author: *gian.debortoli@aalto.fi.*

short filters to enhance the time-frequency features already present in the physical space. In small, dry spaces, this is not the case. Reverberators might need to be used to solve the lack of energy in the natural reverberation. In-line systems use microphones close to the stage musicians and loudspeakers close to the audience. Due to this positioning they favor the diffuse-field assumption, which is not demonstrated to be valid for small, dry spaces or short measurement distances [19], [20].

The stability analysis for the two topologies is formally the same, but due to the transducer positions, the installation space plays a crucial role in deciding whether the diffuse-field assumption is valid. When the transducers are installed in large concert halls with enough distance between each other the assumption is considered valid [13], [21] and the statistical GBI estimation method is suitable. When those conditions are not met, only the deterministic method is feasible, but it analyzes the feedback loop in the frequency domain, not considering how the energy in the feedback paths is distributed over time. In the literature, several techniques to improve the stability threshold are discussed [14], [22], [23], [24], [25], but their effectiveness depends on the how the feedback energy is distributed between direct, early, and late transmissions, which could be inferred from system topology. Neither GBI estimation methods offer cues on which DSP technique is suitable to improve the stability threshold based on the specific installation.

This work studies the case of a medium-sized, dry venue. The main objectives of the study are to analyze the individual contributions of direct, early, and late components of the feedback RIRs to the overall limit of stability and to consider how to improve the limit with known techniques depending on the system topology.

The paper is organized as follows. Section 2 discusses the stability analysis and the GBI estimation. Section 3 describes the venue and RES setup considered in this study and the data pre-processing methodology. Section 4 presents the GBI estimation from different time-frequency slices of the feedback paths and discusses the use of stability-improvement techniques based on the results. Section 5 concludes the study.

2. Stability

For a typical RES with n_{M} microphones and n_{L} loudspeakers, $\mathbf{H}(t) \in \mathbb{R}^{n_{\mathrm{M}} \times n_{\mathrm{L}}}$ is the matrix of feedback RIRs from the system loudspeakers to the system microphones, and $\mathbf{V}(t) \in \mathbb{R}^{n_{\mathrm{L}} \times n_{\mathrm{M}}}$ is the matrix of DSP impulse responses (IRs), where t is the time variable. The corresponding frequency response functions (FRF) are $\mathbf{H}(e^{\jmath\omega}) \in \mathbb{C}^{n_{\mathrm{M}} \times n_{\mathrm{L}}}$ and $\mathbf{V}(e^{\jmath\omega}) \in \mathbb{C}^{n_{\mathrm{L}} \times n_{\mathrm{M}}}$, respectively, where e is Euler's number, $\jmath$ is the imaginary operator, and ω is the frequency variable. The real-valued system gain μ controls the output power of the loudspeakers. According to the generalized Nyquist stability criterion [16], the stability of the system is defined by the open feedback-loop matrix

$$\mathbf{O}(e^{\jmath\omega}) = \mu\mathbf{H}(e^{\jmath\omega})\mathbf{V}(e^{\jmath\omega}), \tag{1}$$

which can be diagonalized with eigenvalue decomposition [10]

$$\mu\mathbf{\Lambda}(e^{\jmath\omega}) = \mathbf{Q}^{-1}(e^{\jmath\omega})\mathbf{O}(e^{\jmath\omega})\mathbf{Q}(e^{\jmath\omega}), \tag{2}$$

where the diagonal matrix $\mathbf{\Lambda}(e^{\jmath\omega}) \in \mathbb{C}^{n_{\mathrm{M}} \times n_{\mathrm{M}}}$ and the unitary matrix $\mathbf{Q}(e^{\jmath\omega}) \in \mathbb{C}^{n_{\mathrm{M}} \times n_{\mathrm{M}}}$ contain the eigenvalues $\left\{\Lambda_{i,i}(e^{\jmath\omega})\right\}$ and the eigenvectors of the system, respectively. The decomposition should be applied at each frequency value, and the eigenvalues should be joined using continuity criteria, obtaining the characteristic functions of the system [13]. Then stability is analyzed from the Nyquist plot of each characteristic function scaled by μ [16]. If the Nyquist plot of any scaled characteristic function encircles the point $1 + \jmath 0$ in the complex plane, then the system is unstable for that value of μ [13].

2.1. Deterministic approach

From in-situ measurements of $\mathbf{H}(n)$ and $\mathbf{V}(n)$, where n is the discrete time variable, $\mathbf{H}(e^{\jmath\omega_k})$ and $\mathbf{V}(e^{\jmath\omega_k})$ are found by discrete Fourier transform (DFT), where ω_k is the discrete frequency at the k^{th} frequency bin. $\mathbf{O}(e^{\jmath\omega_k})$ can thus be obtained for any specific installation and the eigenvalue decomposition is then applied per frequency bin. Instead of retrieving and analyzing the characteristic functions, the GBI is estimated using either

$$\mu_{\max} = \left(\max_{i,\omega_k} \left|\Lambda_{i,i}(e^{\jmath\omega_k})\right|\right)^{-1}, \tag{3}$$

or

$$\mu_{\max} = \left(\max_{i,\omega_k} \Re\left(\Lambda_{i,i}(e^{\jmath\omega_k})\right)\right)^{-1}, \tag{4}$$

where $|\cdot|$ is the absolute value and $\Re(\cdot)$ is the real part. Equations (3) and (4) are based on sufficient but not necessary conditions for stability: they impose a higher threshold on μ such that either the absolute value or the real part of all eigenvalues is lower than 1, ensuring that the Nyquist plot of the characteristic functions cannot encircle the point $1 + \jmath 0$. They provide close estimates while maintaining a small margin from the true stability limit, as in reality the absolute value or the real part of some eigenvalues might be greater than 1 without causing instability [13].

2.2. Statistical approach

The real and imaginary parts of a FRF between distant points in a large concert hall, verifying the diffuse-field assumption, are drawn from the zero-mean Gaussian distribution with known variance σ^2 [21]. In such a case, $\mathbf{H}(e^{\jmath\omega})$ is rotationally invariant, thus, if $\mathbf{V}(e^{\jmath\omega})$ is unitary, the real and imaginary parts of $\mathbf{O}(e^{\jmath\omega})$ are also zero-mean Gaussian distributed [13] with the same variance σ^2. When these conditions are verified, the probability of a RES being unstable can be estimated as the probability of $\mathbf{H}(e^{\jmath\omega_k})$ having either a magnitude or a real part greater than unity for any frequency bin [13]:

$$\mathrm{P}_{\mathrm{inst}}(\mu) = \mathrm{P}\big(\max_{\omega_k} f\big(\mathbf{H}(e^{\jmath\omega_k})\big) > 1\big) \tag{5}$$

where $\mathrm{P}(\cdot)$ indicates probability and $f(\cdot)$ is equivalent to $|\cdot|$ or $\Re(\cdot)$, based on whether the analysis refers to Eq. (3) or (4). In this ideal condition, $\mathrm{P}_{\mathrm{inst}}(\mu)$ depends entirely on σ^2. The GBI can then be estimated, for example, as the value $\mu_{0.5} : \mathrm{P}_{\mathrm{inst}}(\mu_{0.5}) = 0.5$ [13]. A lower gain value, as $\mu_{0.05} : \mathrm{P}_{\mathrm{inst}}(\mu_{0.05}) = 0.05$ [14], ensures a low probability of instability.

In reality, $\mathbf{H}(e^{\jmath\omega})$ vary over time [26]. In the deterministic approach, the eigenvalue decomposition should be applied continuously. Although Eq. (4) produces a closer estimate of the true GBI, while Eq. (3) is more robust to time variation, neither of them can guarantee stability at all time instants. The original formulation of the statistical approach assumes time-invariant $\mathbf{H}(e^{\jmath\omega})$ [13]. In this study, a hybrid approach will be considered, making use of both Eqs. (4) and (5).

3. Case-study setup

This work considers a medium-sized concert venue optimized for amplified live music. The space is acoustically dry and has a different geometry compared to common performance venues. Its volume is 800 m^3 and its reverberation time averaged over the 500 Hz and 1 kHz octave bands is 0.50 s. The RES was installed to support occasional non-amplified performances. Fig. 1a shows a floor plan of the venue with boxes indicating the positions of the RES microphones (green) and loudspeakers (blue) and arrows indicating their orientation. The six microphones are concentrated around the stage area while the 40 loudspeakers are distributed across the entire space. Due to this positioning, the system's topology is not clearly defined, as the loudspeakers close to the stage follow a regenerative setup with respect to the microphone, while the far loudspeakers follow an in-line setup. All transducers are installed just below the ceiling, which is 3 m high. The measured $\mathbf{H}(n)$ are available online [20]. $\mathbf{H}(n)$ was first cleaned from measurement noise before the direct-sound arrival time t_d and after the time t_n, at which the root-mean-squared amplitudes of the RIR and the noise were estimated to be equal. This step was performed by setting to zero all samples before $t_d - 3$ ms and after t_n for each RIR individually.

$\mathbf{H}(e^{\jmath\omega_k}) = \mathcal{F}(\mathbf{H}(n))$, where $\mathcal{F}(\cdot)$ is the DFT, was then normalized according to

$$\mathbf{H}_{\mathrm{norm}}(e^{\jmath\omega_k}) = \frac{\mathbf{H}(e^{\jmath\omega_k})}{\max_{\omega_k,m}\rho(\mathbf{H}(e^{\jmath\omega_k})\mathbf{U}_m)}, \tag{6}$$

where $\rho(\cdot)$ is the spectral radius and $\mathbf{U}_m$ with $m = 1,\ldots,M$ is the m^{th} realization of an element of the Stiefel manifold $S_{n_\mathrm{M}}(\mathbb{R}^{n_\mathrm{L}})$. This normalization guarantees that, if $M \to \infty$, $\mu_{\max}$ as per Eq. (3) is no lower

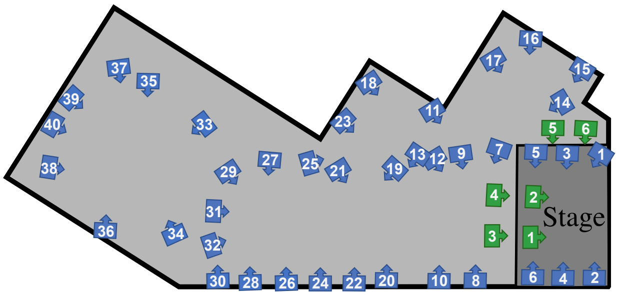

(a) Microphone and loudspeaker positions of the RES in a top view of the venue. Positions and orientations are indicative and not accurately measured.

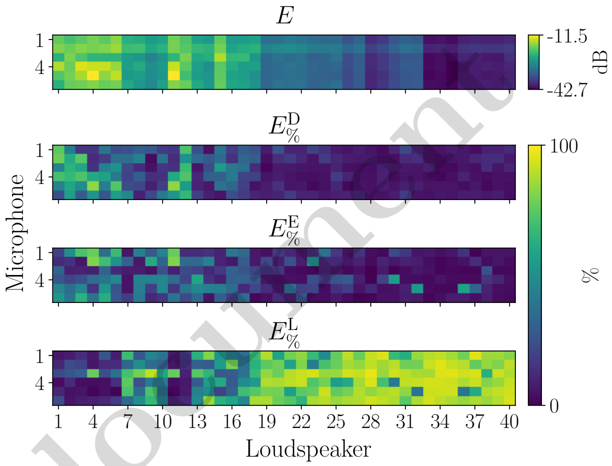

(b) Top to bottom: energy E of $\mathbf{H}^{\mathrm{C}}(n)$, and energy percentages $E^{\mathrm{D}}_{\%}$, $E^{\mathrm{E}}_{\%}$, and $E^{\mathrm{L}}_{\%}$ of $\mathbf{H}^{\mathrm{D}}(n)$, $\mathbf{H}^{\mathrm{E}}(n)$, and $\mathbf{H}^{\mathrm{L}}(n)$, respectively, relative to E.

Figure 1: RES setup and energy balance in the feedback loop.

than 0 dB for any DSP matrix drawn from $S_{n_\mathrm{M}}(\mathbb{R}^{n_\mathrm{L}})$, and as a consequence also as per Eq. (4). In this work, $M = 1000$. When substituted to $\mathbf{V}(e^{\jmath\omega_k})$, $\mathbf{U}_m$ is representative of an energy-preserving mixing matrix. That is demonstrated by considering the squared spectral norm of the right multiplication of $\mathbf{U}_m$ with any vector $\boldsymbol{v} \in \mathbb{R}^{n_\mathrm{M}}$

$$\begin{aligned}\|\mathbf{U}_m\boldsymbol{v}\|_2^2 &= (\mathbf{U}_m\boldsymbol{v})^T(\mathbf{U}_m\boldsymbol{v}) = \boldsymbol{v}^T\mathbf{U}_m^T\mathbf{U}_m\boldsymbol{v} = \\ &= \boldsymbol{v}^T\boldsymbol{v} = \|\boldsymbol{v}\|_2\end{aligned} \tag{7}$$

3.1. Feedback energy

To analyze the effect of direct path, early reflections, and late reverberation on the stability of the system, multiple time slices of each element of the complete RIRs $\mathbf{H}^{\mathrm{C}}(n) = \mathcal{F}^{-1}\big(\mathbf{H}_{\mathrm{norm}}(e^{\jmath\omega_k})\big)$ were considered separately.

The direct power transmission $\mathbf{H}^{\mathrm{D}}(n)$ was obtained by cutting from $t_d - 3$ ms to $t_d + 5$ ms. The early power transmission $\mathbf{H}^{\mathrm{E}}(n)$ spanned from $t_d + 5$ ms to the mixing time t_m, estimated as the time in which the short-time sample distribution of $\mathbf{H}^{\mathrm{C}}(n)$ converged to a zero-mean Gaussian distribution [27]. The late power transmission $\mathbf{H}^{\mathrm{L}}(n)$ spanned from t_m to t_n.

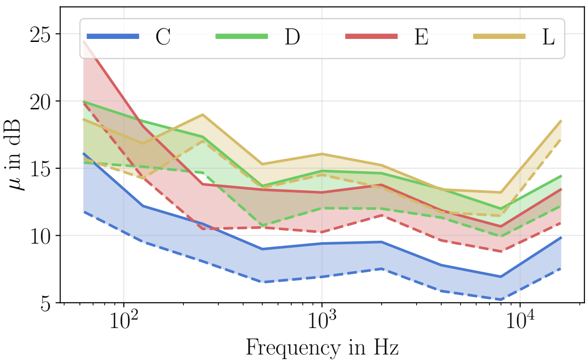

Figure 2: $\mu_{0.5}$ (solid) and $\mu_{0.05}$ (dashed) estimates for $\mathbf{H}^{\mathrm{C}}(n)$ (blue), $\mathbf{H}^{\mathrm{D}}(n)$ (green), $\mathbf{H}^{\mathrm{E}}(n)$ (red), and $\mathbf{H}^{\mathrm{L}}(n)$ (yellow). The areas emphasize the variation of the gain margin with octave band.

The topmost pane of Fig. 1b shows the energy E of $\mathbf{H}^{\mathrm{C}}(n)$. The remaining panes illustrate the energy of $\mathbf{H}^{\mathrm{D}}(n)$, $\mathbf{H}^{\mathrm{E}}(n)$, and $\mathbf{H}^{\mathrm{L}}(n)$, expressed as a percentage of $\mathbf{H}^{\mathrm{C}}(n)$. They are marked by $E^{\mathrm{D}}_{\%}$, $E^{\mathrm{E}}_{\%}$, and $E^{\mathrm{L}}_{\%}$, respectively. Loudspeakers 1 to 6, 11, and 12 contribute the most energy to $\mathbf{H}^{\mathrm{C}}(n)$, mainly due to direct and early transmissions resulting from their proximity and orientation to the stage microphones. Loudspeakers 7 to 10 and 13 to 18 represent the second degree of contribution to $\mathbf{H}^{\mathrm{C}}(n)$, with energy almost equally distributed between direct, early, and late transmissions. Lastly, loudspeakers 19 to 40 transmit little energy, mostly concentrated in the late transmission.

4. Analysis

First, $\mathbf{H}^{\mathrm{C}}(e^{\jmath\omega_k})$, $\mathbf{H}^{\mathrm{D}}(e^{\jmath\omega_k})$, $\mathbf{H}^{\mathrm{E}}(e^{\jmath\omega_k})$, and $\mathbf{H}^{\mathrm{L}}(e^{\jmath\omega_k})$ were obtained using a DFT with $K = 2f_{\mathrm{s}}$ frequency bins for high frequency resolution. A realization of $\mathbf{U}_m$ was drawn from $S_{n_{\mathrm{M}}}(\mathbb{R}^{n_{\mathrm{L}}})$ and used as DSP matrix. The eigenvalues of the open feedback-loop matrix were obtained for each case using Eqs. (1) and (2) for $\mu = 0\,\mathrm{dB}$ and grouped in octave bands. In each octave band, $\mu_{\max}$ was computed according to Eq. (4).

Due to the high contribution of direct and early components to the overall feedback energy, $\mathbf{H}e^{\jmath\omega_k}$ is not rotationally invariant, and thus a specific choice of the matrix $\mathbf{U}_m$ is not representative of the average stability limit over the ensemble of possible realizations of $S_{n_{\mathrm{M}}}(\mathbb{R}^{n_{\mathrm{L}}})$. Thus, the process was repeated for $M = 1000$ realizations of $\mathbf{U}_m$ using Monte Carlo simulations.

From the distribution of the $\mu_{\max}$ values, $\mu_{0.5}$ and $\mu_{0.05}$ were estimated as the 0.5 and the 0.05 quantiles of the data, respectively. The choice of the simulation number M was driven by the inspection of the estimands over cumulative trials, which converged for the chosen value in all octave bands.

Figure 2 presents the results of the Monte Carlo simulations, depicting $\mu_{0.5}$ and $\mu_{0.05}$ estimates in octave bands as solid and dashed lines, respectively. The area between the two curves emphasizes the variation of the safety margin in frequency. The colors separate the four inspected cases: $\mathbf{H}^{\mathrm{C}}(n)$ in blue, $\mathbf{H}^{\mathrm{D}}(n)$ in green, $\mathbf{H}^{\mathrm{E}}(n)$ in red, and $\mathbf{H}^{\mathrm{L}}(n)$ in yellow.

$\mathbf{H}^{\mathrm{C}}(n)$ shows the lowest $\mu_{0.5}$ estimates in each octave band, which is expected since it carries all the feedback energy. Between the remaining three cases, the $\mu_{0.5}$ estimates are similar with the lowest values corresponding to $\mathbf{H}^{\mathrm{E}}(n)$ and the highest to $\mathbf{H}^{\mathrm{L}}(n)$ in most octave bands. The trend is opposite in the lower frequency range.

The safety margin is almost constant over frequency for all cases. $\mathbf{H}^{\mathrm{C}}(n)$ and $\mathbf{H}^{\mathrm{D}}(n)$ present similar margins, $\mathbf{H}^{\mathrm{E}}(n)$ a bit larger, and $\mathbf{H}^{\mathrm{L}}(n)$ a bit narrower. $\mu_{0.5}$ and $\mu_{0.05}$ estimates decrease with increasing frequency for all curves, but increase in the highest octave band.

Overall, Fig. 2 shows that the complete-RIRs GBI estimates are not fully represented by any of the time slices individually, but the main contributions come from direct and late transmissions at low frequencies and from direct and early transmissions at mid-high frequencies.

4.1. Regenerative and in-line systems

To analyze the two RES topologies, two new RES setups were considered by reducing the number of loudspeakers from the default based on the ratio between $E^{\mathrm{D}}_{\%} + E^{\mathrm{E}}_{\%}$ to $E^{\mathrm{L}}_{\%}$. Loudspeakers 1 to 6, 11, and 12 formed a subset that simulated a regenerative system, while loudspeakers 19 to 40 formed a subset that simulated an in-line system. Loudspeakers 7 to 10 and 13 to 18 were neglected, as they are expected to produce a similar trend as seen in Fig. 2. The RIR matrices of both setups were obtained by setting to zero all the columns of $\mathbf{H}_{\mathrm{norm}}(e^{\jmath\omega_k})$ not included in the respective loudspeaker subsets. Both matrices were time sliced according to the description in Sec. 3.1 and the Monte Carlo simulation protocol was repeated using the same realizations of $\mathbf{U}_m$.

Figure 3 shows the results of the simulations for regenerative (left) and in-line (right) setups. The regenerative system shows that late energy transmission has less influence on system stability than direct and early. For the in-line system, instead, the estimations can be almost fully determined by considering only the late energy as the direct and early transmissions are negligible. When comparing the curves of the two sub-systems, the regenerative system shows lower stability thresholds than the in-line, which was expected as the loudspeakers chosen for the regenerative setup are the ones carrying most of the energy in Fig. 1b.

By comparing Figs. 2 and 3, both sub-systems show $\mu_{0.5}$ estimates higher than the full system. The regenerative system shows values for $\mathbf{H}^{\mathrm{C}}(n)$ close to the full system due to the direct and early transmissions being almost equal for the full setups. The in-line system shows higher estimates of $\mu_{0.5}$ and $\mu_{0.05}$ for $\mathbf{H}^{\mathrm{C}}(n)$ than the full system because the feedback component defining the stability limit is the late transmission in correspondence of low-energy RIRs. The $\mu_{0.5} - \mu_{0.05}$

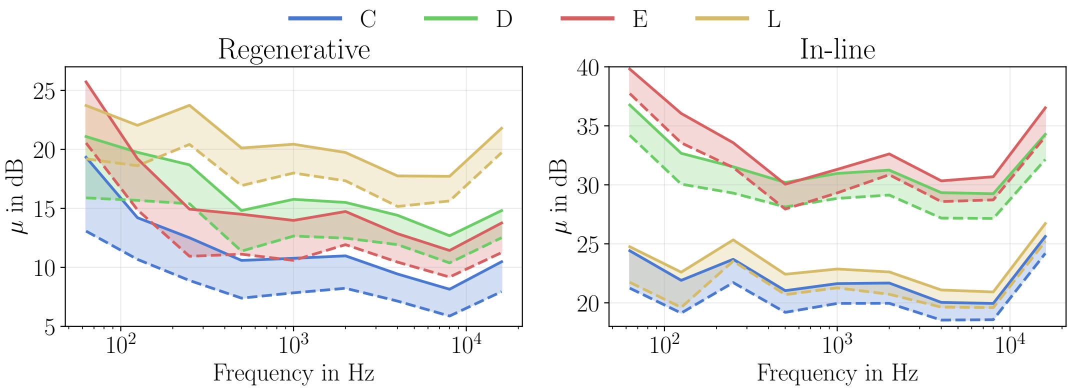

Figure 3: $\mu_{0.5}$ (solid) and $\mu_{0.05}$ (dashed) estimates for $\mathbf{H}^{\mathrm{C}}(n)$ (blue), $\mathbf{H}^{\mathrm{D}}(n)$ (green), $\mathbf{H}^{\mathrm{E}}(n)$ (red), and $\mathbf{H}^{\mathrm{L}}(n)$ (yellow). The areas emphasize the variation of the gain margin with octave band. The left pane refers to the setup using only the loudspeakers 1 to 6, 11, and 12. The right pane to the setup using only the loudspeakers 19 to 40.

margins for the regenerative system are identical to the full system, while the in-line system shows narrower margins stating a faster transition from stable to unstable conditions with increasing system gain.

4.2. Stability threshold improvement

Typical techniques for improving the stability threshold include [18]: the increase of sample decorrelation, either between system channels or in time, and feedback cancelation. They have different working principles, as the first approach smooths the feedback FRFs towards the mean loop gain by increasing the stochasticity of the time-frequency samples, while the second one takes advantage of predictable time samples to minimize the feedback.

A larger channel count increases decorrelation between channels when the transducers are well spaced in a large hall, capturing different modes and reflection patterns [22]. In a small room, instead, microphones and loudspeakers will inevitably present coherent FRFs, thus increasing the transducer density will not effectively benefit channel decorrelation. In a dry and small spaces, most of the feedback energy is concentrated in the early parts of the feedback RIRs, which present high coherence in time [26]. Thus, feedback cancellation is a suitable solution which suppresses the portion of feedback energy attributed to deterministic reflections [25]. Canceling filters might not work, instead, in large spaces where the feedback RIRs have high energy in the late part, which has stochastic behavior [28]. Time variation could solve both cases, but, since it works by distributing feedback energy of each frequency bin to the neighboring ones, it works well only for well equalized system, with equal energy in all frequency bands, and if the feedback FRF variance σ^2 is small then its contribution might be minimal [12].

5. Conclusions

This work explored the contributions of the feedback components to the stability of a reverberation enhancement system installed in a dry, medium-sized concert venue. Direct path, early reflections, and late reverberation in the feedback paths have been isolated, and the system stability threshold has been estimated for each component in octave bands. Additionally, the system setup was modified to show different RES topologies and how the contributions behave accordingly. The results show that when the system includes loudspeakers both far and close to the microphones, stability is strongly affected by all three time components of the feedback paths in all octave bands. Direct and late reflections dominate at low frequencies, while the early and late reverberation are most influential at mid and high frequencies. When the system's loudspeakers are all close to the microphones, the late reverberation is negligible in the stability analysis; when, instead, the loudspeakers are all far away from the microphones, the stability can be almost fully estimated by analyzing only the late reverberation. These observations led to a discussion on the suitability of stability-improvement techniques based on the system topology.

6. Acknowledgments

The work of the first author was funded by the Research Council of Finland (Project No. 357391).

References

[1] M. A. Poletti, "Active Acoustic Systems for the Control of Room Acoustics," *Building Acoustics*, vol. 18, no. 3-4, pp. 237–258, Dec. 2011.

[2] A. Krokstad, "Electroacoustic means of controlling auditorium acoustics," *Appl. Acoust.*, vol. 24, no. 4, pp. 275–288, Jan. 1988.

[3] T. Lokki, J. Pätynen, T. Peltonen, and O. Salmensaari, "A Rehearsal Hall with Virtual Acoustics for Symphony Orchestras," in *Proc. 126th Audio Eng. Soc. Conv.*, Munich, Germany, 2009.

[4] C. Hough, N. Boulter, and S. Tait, "The use of electrocoustic enhancement systems in the design of orchestral rehearsal rooms," *J. Acoust. Soc. Am.*, vol. 157, no. 4 Supplement, Apr. 2025.

[5] W. Woszczyk, T. Beghin, M. de Francisco, and D. Ko, "Recording Multichannel Sound Within Virtual Acoustics," in *Proc. 127th Audio Eng. Soc. Conv.*, New York, NY, USA, 2009.

[6] G. Grazioli, V. Baran, K. Y.-Y. Zhang, A. Aydin, and W. Woszczyk, "Preliminary evaluation of a sound system employing a cancelling auralizer for producing virtual rooms in a modern recording studio," in *Proc. I3DA*, Bologna, Italy, 2023, pp. 1–7.

[7] R. Guelke, "Assisted Reverberation in an Outdoor Environment," *Acustica*, vol. 38, no. 5, pp. 335–337, 1977.

[8] S. Barbar, "Inside Out - Time Variant Electronic Acoustic Enhancement Provides the Missing Link for Acoustic Music Outdoors," in *Proc. 127th Audio Eng. Soc. Conv.*, New York, NY, USA, 2009.

[9] R. V. Waterhouse, "Theory of Howlback in Reverberant Rooms," *J. Acoust. Soc. Am.*, vol. 37, no. 5, pp. 921–923, May 1965.

[10] M. Ohsmann, "Analyse Von Mehrkanalanlagen," *Acustica*, vol. 70, no. 4, pp. 233–246, 1990.

[11] G. De Bortoli, G. Dal Santo, K. Prawda, T. Lokki, V. Välimäki, and S. J. Schlecht, "Differentiable active acoustics: Optimizing stability via gradient descent," in *Proc. 27th Int. Conf. DAFx*, Guilford, UK, 2024, pp. 254–261.

[12] M. R. Schroeder, "Improvement of Acoustic-Feedback Stability by Frequency Shifting," *J. Acoust. Soc. Am.*, vol. 36, no. 9, pp. 1718–1724, Sep. 1964.

[13] M. A. Poletti, "The Stability of Single and Multichannel Sound Systems," *Acta Acust. un. Acust.*, vol. 86, no. 1, pp. 163–178, 2000.

[14] S. J. Schlecht and E. A. P. Habets, "The stability of multichannel sound systems with time-varying mixing matrices," *J. Acoust. Soc. Am.*, vol. 140, no. 1, pp. 601–609, Jul. 2016.

[15] H. Nyquist, "Regeneration theory," *Bell Syst. Tech. J.*, vol. 11, no. 1, pp. 126–147, Jan. 1932.

[16] A. G. J. MacFarlane and I. Postlethwaite, "The generalized Nyquist stability criterion and multivariable root loci," *Int. J. Control*, vol. 25, no. 1, pp. 81–127, Jan. 1977.

[17] M. R. Schroeder, "Statistical Parameters of the Frequency Response Curves of Large Rooms," *J. Audio Eng. Soc.*, vol. 35, no. 5, pp. 299–306, May 1987.

[18] W. J. Cassidy et al., "Active acoustic enhancement systems: A review," *J. Acoust. Soc. Am.*, vol. 159, no. 4, pp. 3533–3557, Apr. 2026.

[19] M. R. Schroeder and K. H. Kuttruff, "On Frequency Response Curves in Rooms. Comparison of Experimental, Theoretical, and Monte Carlo Results for the Average Frequency Spacing between Maxima," *J. Acoust. Soc. Am.*, vol. 34, no. 1, pp. 76–80, Jan. 1962.

[20] G. De Bortoli, K. Prawda, P. Coleman, and S. J. Schlecht, *DataRES*, 2025. DOI: `10.5281/zenodo.15737243`.

[21] M. R. Schroeder, "Frequency-Correlation Functions of Frequency Responses in Rooms," *J. Acoust. Soc. Am.*, vol. 34, no. 12, pp. 1819–1823, Dec. 1962.

[22] D. Griesinger, "Improving room acoustics through time-variant synthetic reverberation," in *Proc. 90th Audio Eng. Soc. Conv.*, Paris, France, 1991.

[23] U. P. Svensson, "On reverberation enhancement in auditoria," phd, Chalmers Univ. of Technology, Göteborg, 1994.

[24] H. Miyazaki, T. Watanabe, S. Kishinaga, and F. Kawakami, "Active Field Control (AFC): Reverberation Enhancement System Using Acoustical Feedback Control," in *Proc. 115th Audio Eng. Soc. Conv.*, New York, NY, USA, 2003.

[25] J. S. Abel, E. F. Callery, and E. K. Canfield-Dafilou, "A Feedback Canceling Reverberator," in *Proc. 21st Int. Conf. DAFx*, Aveiro, Portugal, 2018, pp. 100–106.

[26] K. Prawda, S. J. Schlecht, and V. Välimäki, "Short-time coherence between repeated room impulse response measurements," *J. Acoust. Soc. Am.*, vol. 156, no. 2, pp. 1017–1028, Aug. 2024.

[27] J. S. Abel and P. Huang, "A Simple, Robust Measure of Reverberation Echo Density," in *Proc. 121st Audio Eng. Soc. Conv.*, San Francisco, CA, USA, 2006.

[28] J. S. Abel et al., "Recreation of the acoustics of Hagia Sophia in Stanford's Bing Concert Hall for the concert performance and recording of Cappella Romana," in *Proc. ISRA*, Toronto, Canada, 2013, pp. 1–13.